

# Effect of high SWNT content on the room temperature mechanical properties of fully dense 3YTZP/SWNT composites

R. Poyato<sup>\*1</sup>, A. Gallardo-López<sup>2</sup>, F. Gutiérrez-Mora<sup>2</sup>, A. Morales-Rodríguez<sup>2</sup>,  
A. Muñoz<sup>2</sup> y A. Domínguez-Rodríguez<sup>2</sup>

1. *Inst. Ciencia de Materiales de Sevilla (CSIC-Univ. Sevilla), Avda. Américo Vespucio 49, 41092 Sevilla*
2. *Dep. Física de la Materia Condensada, Univ. de Sevilla, apdo. 1065, 41012 Sevilla*

## Abstract

This paper is devoted to correlate the microstructure and room temperature mechanical properties of single-wall carbon nanotube (SWNT) reinforced 3 mol% yttria stabilized tetragonal zirconia with high SWNT content (2.5, 5 and 10 vol%). Fully dense composites were prepared by using a combination of aqueous colloidal powder processing and Spark Plasma Sintering. SWNTs were located at the ceramic grain boundaries and they were not damaged during the sintering process. The weak interfacial bonding between SWNTs and ceramic grains together with the detachment of SWNTs within thick bundles have been pointed out as responsible for the decrease of hardness and fracture toughness of the composites in comparison with the monolithic 3YTZP ceramic

**Keywords:** composites; carbon nanotubes; processing; Spark Plasma Sintering; mechanical properties

\*Corresponding author. E-mail address: [rosalia.poyato@icmse.csic.es](mailto:rosalia.poyato@icmse.csic.es)

Phone number: +34 954 48 95 34

FAX number: +34 954 46 06 65

## 1. Introduction

During the last decade, there has been an increasing interest in the development of advanced ceramic matrix composites containing carbon nanotubes (CNTs)<sup>1-3</sup>, as it is expected that some of the attractive properties of the CNTs<sup>4,5</sup> (high Young's modulus, high tensile strength, high electrical conductivity or good thermal conductivity) will be transferred to the resulting composites. However, up to date, the positive effects of CNTs addition on the mechanical properties of ceramic matrix composites are still matter of debate. Whereas some groups reported enhancements in properties as fracture toughness or creep resistance<sup>6-10</sup>, other authors found no improvements or even a detrimental effect of the CNTs addition<sup>11-14</sup>.

The disparity of results can be related to the different processing methods used to prepare the composites, giving place to very different microstructures or not completely densified composites. The key points in the processing of these type of composites are, on one hand, a homogeneous dispersion of CNTs in the ceramic matrix together with a good interfacial bonding between both materials, and on the other, a high densification of the material. Several approaches, including different powder processing and sintering methods have been proposed in literature. Physical mixing under wet conditions by ultrasonication, ball milling or attrition milling has been conducted to disperse CNTs into alumina or zirconia powders<sup>2,6,8-11</sup>. Other approaches as colloidal processing including heterocoagulation, use of dispersants or charge stabilization have been also discussed in literature<sup>13-17</sup>. Recently, the in-situ growth of multi-wall carbon nanotubes (MWNT) onto alumina<sup>18</sup> or zirconia<sup>19</sup> particles was reported as a good approach to obtain a good dispersion of the CNTs in the ceramic matrix and a high density after consolidation by spark plasma sintering (SPS).

1  
2 Among the published studies on ceramic matrix composites in recent years  
3 several works were devoted to the study of zirconia-based composites, as the superior  
4 mechanical properties and good ionic conductivity of yttria-doped zirconia make this  
5 ceramic a technologically interesting material for a wide range of applications such as  
6 structural material, solid oxide fuel cells or oxygen sensors<sup>20-22</sup>.  
7  
8  
9

10  
11 Most of the studies about CNTs reinforced zirconia reported heterocoagulation  
12 or use of dispersants for the processing of the composite powder<sup>13-15,23,24</sup>, sometimes  
13 combined with other techniques such as slip-casting<sup>14</sup> or spray drying<sup>25</sup>. Regarding the  
14 densification step, hot pressing<sup>13,25</sup> or conventional<sup>14</sup> sintering were used by some  
15 authors. Garmendia *et al*<sup>14</sup> reported a colloidal processing route based on the strong  
16 attractive interaction of the MWNT and the 3 mol% yttria-doped zirconia (3YTZP)  
17 powder by heterocoagulation, using poly(ethylenimine) (PEI) as cationic dispersant.  
18 After slip casting and conventional sintering they obtained composites with 96% of the  
19 theoretical density. In their study, significant improvements in hardness or fracture  
20 toughness were not achieved. Zhou *et al*<sup>25</sup> combined heterocoagulation using  
21 polyacrylate acid (PAA) with spray drying to obtain the 3YTZP/MWNT composite  
22 powder. Fully densified composites were not obtained after hot-pressing the composites  
23 (98% of the theoretical density for composites with 0.5 and 1 wt% MWNT). However,  
24 increases in flexural strength and fracture toughness were reported up to 1.0 wt%  
25 MWNT.  
26  
27  
28  
29  
30  
31  
32  
33  
34  
35  
36  
37  
38  
39  
40  
41  
42  
43  
44  
45  
46  
47

48 Among the reported studies on CNT/3YTZP composites, highly densified  
49 samples were only obtained in studies using SPS<sup>19,23,24</sup>. Nevertheless, a decrease of  
50 hardness in the composites when compared with the monolithic ceramic, even when  
51 they are fully densified, and an increase of fracture toughness only for low percentages  
52 of CNTs<sup>11,15,19,23-25</sup> have been reported in most of these studies. Recently, Mazaheri *et*  
53  
54  
55  
56  
57  
58  
59  
60  
61  
62  
63  
64  
65

1  
2  
3  
4  
5  
6  
7  
8  
9  
10  
11  
12  
13  
14  
15  
16  
17  
18  
19  
20  
21  
22  
23  
24  
25  
26  
27  
28  
29  
30  
31  
32  
33  
34  
35  
36  
37  
38  
39  
40  
41  
42  
43  
44  
45  
46  
47  
48  
49  
50  
51  
52  
53  
54  
55  
56  
57  
58  
59  
60  
61  
62  
63  
64  
65  
*al*<sup>8,9</sup> reported an increase of fracture toughness on nearly fully dense 3 mol% yttria-doped zirconia reinforced with 0.5-5 wt% MWNT with no detrimental effect on hardness. These composites were prepared by a combination of attrition milling and SPS.

Up to date, most of the investigations focused on MWNT reinforced yttria-doped zirconia, however, the study of processing and mechanical properties of single wall carbon nanotube (SWNT) reinforced yttria stabilized zirconia composites is still a challenge. SWNT present better mechanical properties than MWNT as it is possible to avoid the inter-wall sliding that can take place in MWNT, with inner graphitic walls being extracted from outer walls in a “sword and sheath” failure<sup>6,26</sup>. However, SWNT tend to agglomerate easily due to Van der Waals interactions, which complicate the composites processing. Recently, Shin and Hong<sup>27</sup> reported on the processing and microstructure of SWNT reinforced yttria stabilized zirconia composites with promising mechanical and tribological properties. These authors combined the use of dimethylformamide as a solvent to disperse the SWNT in the matrix with SPS to obtain composites with 0.1-1.0 wt% SWNT. Although full densification was not obtained in the whole set of composites, an enhancement of fracture toughness together with an improvement of wear properties was reported.

In recent years, an intense debate on the reliability of different fracture toughness measurement methods to characterize CNT-ceramic matrix composites has taken place<sup>12,23,28-31</sup>. There have been different arguments about the validity of the indentation technique, and some authors have compared the results obtained using this method with the ones obtained with the single edge notched beam (SENB) test. Wang *et al*<sup>12</sup> have shown that cracks are hardly produced in SWNT-Al<sub>2</sub>O<sub>3</sub> composites after Vickers or Hertzian indentation, which would give extremely high fracture toughness

1 values; however, no increase of fracture toughness was obtained from SENB  
2 measurements. An increase of  $K_{IC}$  when increasing the CNT content has been reported  
3 by Cho *et al*<sup>31</sup> and Mazaheri *et al*<sup>9</sup> for MWNT-SiO<sub>2</sub> and MWNT-3YTZP composites,  
4 respectively. Although the absolute values of  $K_{IC}$  measured by Vickers indentation or  
5 SENB test differ (higher values obtained from indentation measurements), a similar  
6 trend was observed when measuring using the two techniques. It seems clear that the  
7 indentation technique should not be used to determine absolute values of  $K_{IC}$  in CNT-  
8 ceramic matrix composites. Nevertheless, it has been proposed that this test could be  
9 useful for assessing relative toughness values in well-densified materials with good  
10 nanoscale dispersion if sufficiently developed cracks are produced<sup>23,31</sup>. In this context,  
11 although the  $K_{IC}$  values obtained from Vickers indentations are not directly comparable  
12 to values in the literature for materials tested with the SENB method, they can be used  
13 to compare different compositions tested in a same study.

14  
15  
16  
17  
18  
19  
20  
21  
22  
23  
24  
25  
26  
27  
28  
29  
30  
31 In this work, 3 mol% yttria doped zirconia matrix composites containing high  
32 SWNT content (2.5, 5 and 10 vol%) were prepared by using a combination of aqueous  
33 colloidal processing and Spark Plasma Sintering. Full densification, together with  
34 homogeneous dispersion of the SWNT throughout the ceramic matrix in the nanoscale,  
35 was obtained. The microstructure of the composites was characterized and the evolution  
36 of their hardness and fracture toughness with SWNT volume fraction was analysed.

## 37 38 39 40 41 42 43 44 45 46 47 48 **2. Experimental procedure**

### 49 50 51 52 53 54 55 56 57 58 59 60 61 62 63 64 65 66 67 68 69 70 71 72 73 74 75 76 77 78 79 80 81 82 83 84 85 86 87 88 89 90 91 92 93 94 95 96 97 98 99 100 101 102 103 104 105 106 107 108 109 110 111 112 113 114 115 116 117 118 119 120 121 122 123 124 125 126 127 128 129 130 131 132 133 134 135 136 137 138 139 140 141 142 143 144 145 146 147 148 149 150 151 152 153 154 155 156 157 158 159 160 161 162 163 164 165 166 167 168 169 170 171 172 173 174 175 176 177 178 179 180 181 182 183 184 185 186 187 188 189 190 191 192 193 194 195 196 197 198 199 200 201 202 203 204 205 206 207 208 209 210 211 212 213 214 215 216 217 218 219 220 221 222 223 224 225 226 227 228 229 230 231 232 233 234 235 236 237 238 239 240 241 242 243 244 245 246 247 248 249 250 251 252 253 254 255 256 257 258 259 260 261 262 263 264 265 266 267 268 269 270 271 272 273 274 275 276 277 278 279 280 281 282 283 284 285 286 287 288 289 290 291 292 293 294 295 296 297 298 299 300 301 302 303 304 305 306 307 308 309 310 311 312 313 314 315 316 317 318 319 320 321 322 323 324 325 326 327 328 329 330 331 332 333 334 335 336 337 338 339 340 341 342 343 344 345 346 347 348 349 350 351 352 353 354 355 356 357 358 359 360 361 362 363 364 365 366 367 368 369 370 371 372 373 374 375 376 377 378 379 380 381 382 383 384 385 386 387 388 389 390 391 392 393 394 395 396 397 398 399 400 401 402 403 404 405 406 407 408 409 410 411 412 413 414 415 416 417 418 419 420 421 422 423 424 425 426 427 428 429 430 431 432 433 434 435 436 437 438 439 440 441 442 443 444 445 446 447 448 449 450 451 452 453 454 455 456 457 458 459 460 461 462 463 464 465 466 467 468 469 470 471 472 473 474 475 476 477 478 479 480 481 482 483 484 485 486 487 488 489 490 491 492 493 494 495 496 497 498 499 500 501 502 503 504 505 506 507 508 509 510 511 512 513 514 515 516 517 518 519 520 521 522 523 524 525 526 527 528 529 530 531 532 533 534 535 536 537 538 539 540 541 542 543 544 545 546 547 548 549 550 551 552 553 554 555 556 557 558 559 560 561 562 563 564 565 566 567 568 569 570 571 572 573 574 575 576 577 578 579 580 581 582 583 584 585 586 587 588 589 590 591 592 593 594 595 596 597 598 599 600 601 602 603 604 605 606 607 608 609 610 611 612 613 614 615 616 617 618 619 620 621 622 623 624 625 626 627 628 629 630 631 632 633 634 635 636 637 638 639 640 641 642 643 644 645 646 647 648 649 650 651 652 653 654 655 656 657 658 659 660 661 662 663 664 665 666 667 668 669 670 671 672 673 674 675 676 677 678 679 680 681 682 683 684 685 686 687 688 689 690 691 692 693 694 695 696 697 698 699 700 701 702 703 704 705 706 707 708 709 710 711 712 713 714 715 716 717 718 719 720 721 722 723 724 725 726 727 728 729 730 731 732 733 734 735 736 737 738 739 740 741 742 743 744 745 746 747 748 749 750 751 752 753 754 755 756 757 758 759 760 761 762 763 764 765 766 767 768 769 770 771 772 773 774 775 776 777 778 779 780 781 782 783 784 785 786 787 788 789 790 791 792 793 794 795 796 797 798 799 800 801 802 803 804 805 806 807 808 809 810 811 812 813 814 815 816 817 818 819 820 821 822 823 824 825 826 827 828 829 830 831 832 833 834 835 836 837 838 839 840 841 842 843 844 845 846 847 848 849 850 851 852 853 854 855 856 857 858 859 860 861 862 863 864 865 866 867 868 869 870 871 872 873 874 875 876 877 878 879 880 881 882 883 884 885 886 887 888 889 890 891 892 893 894 895 896 897 898 899 900 901 902 903 904 905 906 907 908 909 910 911 912 913 914 915 916 917 918 919 920 921 922 923 924 925 926 927 928 929 930 931 932 933 934 935 936 937 938 939 940 941 942 943 944 945 946 947 948 949 950 951 952 953 954 955 956 957 958 959 960 961 962 963 964 965 966 967 968 969 970 971 972 973 974 975 976 977 978 979 980 981 982 983 984 985 986 987 988 989 990 991 992 993 994 995 996 997 998 999 10002.1. Materials Processing

#### 2.1.1 SWNTs acid treatment

1  
2  
3  
4  
5  
6  
7  
8  
9  
10  
11  
12  
13  
14  
15  
16  
17  
18  
19  
20  
21  
22  
23  
24  
25  
26  
27  
28  
29  
30  
31  
32  
33  
34  
35  
36  
37  
38  
39  
40  
41  
42  
43  
44  
45  
46  
47  
48  
49  
50  
51  
52  
53  
54  
55  
56  
57  
58  
59  
60  
61  
62  
63  
64  
65

Commercially available purified SWNT (Carbon Solutions Inc., Riverside, California) were selected as starting material. Acid treatment of the SWNTs was carried out using a mixture of concentrated sulfuric acid (98%) and nitric acid (70%) in the ratio 3:1, with the aim of disentangle and cut the raw SWNTs ropes<sup>16,32</sup>. SWNTs were suspended in the acid mixture for 24 h at room temperature; the suspension was sonicated for 8 h. SWNTs were collected on ~20 nm pore filter membranes and washed with high-purity ethanol several times. The acid-treated SWNTs were then dried on hot plate at 70-80 °C and homogenized in agate mortar.

### 2.1.2 3YTZP-SWNTs powder colloidal processing

3 mol% yttria stabilized tetragonal zirconia powder (3YTZP), with 40 nm particle size and 99% purity, was obtained from a commercial source (Nanostructured and Amorphous Materials Inc., Houston, Texas). Colloidal processing<sup>16</sup> of the composite powders (2.5, 5 and 10 vol% SWNTs) was carried out in aqueous solution of pH 12, where both the SWNTs and the 3YTZP nanoparticle surfaces are negatively charged, using NH<sub>3</sub> to adjust the solution pH. In a first step, independent SWNTs and ceramic powder solutions were prepared and subjected to ultrasonic agitation for 30 min. In a second step, 3YTZP+SWNTs powder blends were dispersed in aqueous solution and subjected to ultrasonic agitation for 30 min, followed by drying on a hot plate while being stirred. Finally, composite powders were homogenized in agate mortar.

By using this colloidal dispersion by charge stabilization we avoid using surfactants that could introduce undesirable impurities which could affect the sintering process and/or composites properties.

### 2.1.3 Spark Plasma Sintering (SPS)

The SPS (Model 515S, SPS Dr Sinter Inc., Kanagawa, Japan) of the composite powders was performed in vacuum in a 15-mm diameter cylindrical graphite die/punch setup, under a uniaxial pressure of 75 MPa at 1250 °C for 5 min. The heating and cooling rates were 300 and 50 °C/min, respectively. For the sake of comparison, monolithic 3YTZP ceramic was sintered using the same conditions. A sheet of graphite paper was placed between the powders and die/punches for easy specimen removal. Temperature was measured by means of an optical pyrometer focused on a bore hole in the middle part of the graphite die. The sintered ceramics of ~15 mm in diameter and ~2 mm in thickness were ground to eliminate the surface carbon.

Density of the composites was determined using the Archimedes' method, using water as the immersion liquid. The theoretical densities of the composites were calculated according to the rule of the mixtures, assuming a density of 1.80 g cm<sup>-3</sup> for SWNTs<sup>3</sup>.

## 2.2. Microstructural and mechanical characterization

Phase identification was carried out using X-ray diffraction (XRD, model D8 Advance A25, Bruker Co., Massachusetts, USA). The Rietveld method was used for quantitative analysis using the FULLPROF program.

Sintered composites were characterized by Raman spectroscopy in order to detect possible damage of SWNTs after sintering. Raman spectra were recorded on fracture surfaces using a dispersive microscope (Horiba Jobin Yvon LabRam HR800, Kyoto, Japan), with a 20-mW He-Ne green laser (532.14 nm), without filter, and with a

1  
2  
3  
4  
5  
6  
7  
8  
9  
10  
11  
12  
13  
14  
15  
16  
17  
18  
19  
20  
21  
22  
23  
24  
25  
26  
27  
28  
29  
30  
31  
32  
33  
34  
35  
36  
37  
38  
39  
40  
41  
42  
43  
44  
45  
46  
47  
48  
49  
50  
51  
52  
53  
54  
55  
56  
57  
58  
59  
60  
61  
62  
63  
64  
65

600 g/mm grating. The microscope used a 100x objective and a confocal pinhole of 100  $\mu\text{m}$ . The Raman spectrometer was calibrated using a silicon wafer.

Microstructural observations of sintered composites were carried out on the fracture and polished surfaces by high-resolution scanning electron microscopy (HRSEM), using a Hitachi S5200 microscope (Hitachi High Technologies America Inc., USA). Polished samples (up to 1  $\mu\text{m}$  diamond paste) were thermally etched at 1150  $^{\circ}\text{C}$  for 20 min in air to reveal the grain boundaries. The morphological parameters equivalent planar diameter,  $d = (4 \times \text{area} / \pi)^{1/2}$  and shape factor,  $F = (\text{perimeter})^2 / 4 \times \text{area}$ , were measured on HRSEM micrographs by using ImageJ software.

Vickers indentation tests were carried out with a diamond Vickers indenter to establish the hardness and fracture toughness at room temperature, under 2 kgf and 10 kgf, respectively. At least 15 valid measurements were carried out on mirror-like finished top surfaces for each sample, in well-separated and randomly selected regions. The crack lengths were measured using a LEICA DCM 3D confocal microscope.

The fracture toughness,  $K_{IC}$ , was calculated by using the equation given by Anstis *et al.*<sup>33</sup>.

$$K_{IC} = 0.016 \left( \frac{E}{H} \right)^{1/2} \left( \frac{P}{c^{3/2}} \right) \quad (1)$$

where  $c$  is the crack length measured from the center of the imprint,  $E$  is the elastic modulus in GPa and  $H$  is the Vickers hardness in GPa, calculated from the indentation load  $P$  and the diagonal of the Vickers imprint  $a$ :

$$H = 1.854 \frac{P}{a^2} \quad (2)$$

### 3. Results and discussion



1  
2  
3  
4  
5  
6  
7  
8  
9  
10  
11  
12  
13  
14  
15  
16  
17  
18  
19  
20  
21  
22  
23  
24  
25  
26  
27  
28  
29  
30  
31  
32  
33  
34  
35  
36  
37  
38  
39  
40  
41  
42  
43  
44  
45  
46  
47  
48  
49  
50  
51  
52  
53  
54  
55  
56  
57  
58  
59  
60  
61  
62  
63  
64  
65

Figure 1 shows the evolution of the shrinkage and temperature as a function of time during heating and stabilization at the sintering temperature for the composites with different SWNTs content. This evolution was recorded *in situ* during the SPS process. It can be observed that sintering takes place mainly for temperatures higher than 850 °C and up to 1200 °C, with a slight density enhancement for temperatures from 1200 °C to 1250 °C. A similar behaviour is observed in all sintered composites, which is in agreement with the full densification measured by the Archimedes method in the three composites (**>99% relative density for the three composites, table 1**).

19  
20  
21  
22  
23  
24  
25  
26  
27  
28  
29  
30  
31  
32  
33  
34  
35  
36  
37  
38  
39  
40  
41  
42  
43  
44  
45  
46  
47  
48  
49  
50  
51  
52  
53  
54  
55  
56  
57  
58  
59  
60  
61  
62  
63  
64  
65

XRD patterns of the sintered specimens are shown in figure 2. In all the samples, it is clear the presence of the tetragonal phase (JCPDS 01-078-1808) as the main one, with a contribution of the monoclinic phase (JCPDS 01-081-1314). Rietveld refinement carried out for the monolithic 3YTZP ceramic pointed out the formation of these two phases, being the major crystalline phase the tetragonal one (92.4%) and the minor phase the monoclinic one (7.6%). An increase of the two main peaks corresponding to the monoclinic phase (at 28.2 and 31.4 °2θ) is clearly observed when increasing the SWNT content. Thus, the transformation of the tetragonal phase to the monoclinic one is clearly favoured by the addition of SWNT. Bocanegra-Bernal *et al*<sup>34</sup> have recently experimentally evidenced such transformation in ZrO<sub>2</sub> for zirconia toughened alumina (ZTA)/0.01 wt% MWNT composites pressureless sintered in air using graphite as bed powder. The increasing effect observed in our results states that it is indeed the presence of carbon nanotubes (SWNTs in this case) which promotes the presence of the monoclinic phase. However, the mechanism of this transformation is still unclear and future work on this subject will be carried out.

56  
57  
58  
59  
60  
61  
62  
63  
64  
65

Figure 3 shows the Raman spectra measured in the sintered composites, as well as in the monolithic 3YTZP ceramic and in the SWNTs. The Raman spectra measured

1  
2  
3  
4  
5  
6  
7  
8  
9  
10  
11  
12  
13  
14  
15  
16  
17  
18  
19  
20  
21  
22  
23  
24  
25  
26  
27  
28  
29  
30  
31  
32  
33  
34  
35  
36  
37  
38  
39  
40  
41  
42  
43  
44  
45  
46  
47  
48  
49  
50  
51  
52  
53  
54  
55  
56  
57  
58  
59  
60  
61  
62  
63  
64  
65

in the composites show characteristic radial breathing mode (RBM) bands near 150–200  $\text{cm}^{-1}$  and G-bands near 1500–1600  $\text{cm}^{-1}$ , which are very similar to the measured ones in the SWNT before processing of the composites. These results clearly demonstrate the presence of SWNTs after SPS. The D-band (centred on 1350  $\text{cm}^{-1}$ ) shows a slight increase, which can be attributed to the formation of disordered graphite and defects in the composites during the SPS process. When comparing the spectra measured in the composites and in the SWNTs, a shift towards higher frequencies is observed in the composites G-band ( $\sim 20 \text{ cm}^{-1}$ ), which has been attributed by different authors to residual stresses in the SWNTs imposed by the constraining ceramic matrix<sup>12,35</sup>. On the other hand, peaks at 165, 260, 320, 465, 610, and 643  $\text{cm}^{-1}$  are observed in the spectra measured in the composites. These peaks correspond to the six Raman bands predicted for theoretical tetragonal zirconia, as has been described by previous authors<sup>36,37</sup>.

HR-SEM micrographs of fracture surface of the composites reinforced with different SWNTs content are presented in figure 4. SWNTs bundles are located on the ceramic grain boundaries and debonded CNTs from the matrix can be observed on the fracture surfaces. The fracture mode is mainly intergranular (grain boundary weakness due to the presence of the SWNTs promotes intergranular fracture along grain boundaries, over transgranular fracture through the grains). SWNTs are well distributed on the ceramic matrix, however, some agglomerates could be observed in the composites (not shown). The presence of these nanotube agglomerates or clusters has been reported by previous authors<sup>10,13,17,23,25</sup>. Recently, Poorteman *et al*<sup>17</sup> found such inhomogeneities in MWNT-ceramic matrix composites even after using aqueous colloidal processing optimizing electrostatic repulsion and conserving the homogeneity by freeze-drying the composite powder. A thermodynamic explanation based on the free

1 volume of isotropic particles and particles with a high aspect ratio, which promotes the  
2 demixion of both phases, was suggested.  
3

4 Figure 5 shows the HR-SEM micrographs of thermally etched polished surfaces  
5 and grain size distribution plots of monolithic 3YTZP ceramic and composite with 5  
6 vol% SWNTs. An equiaxed grain microstructure was found in all the materials (shape  
7 factor around 0.8, table 1). Some holes can be observed (fig. 5(c)), which could  
8 correspond to previous locations of SWNT bundles or agglomerates burned out during  
9 thermal etching in air. While global microstructure presents a mean grain size about 250  
10 nm for all compositions (table 1), areas with larger grain sizes were scarcely observed  
11 (not shown). These zones could be related to monoclinic transformed regions.  
12  
13  
14  
15  
16  
17  
18  
19  
20  
21  
22  
23

24 Some authors have reported a decrease in grain size with increasing SWNT  
25 content, however, this reduction is usually related to a decrease in the density of the  
26 composite<sup>10,13,27</sup>. This fact can be ruled out in this study, since all the processed  
27 composites are fully densified and a clear effect of the SWNT percentage on the mean  
28 grain size is not observed (table 1).  
29  
30  
31  
32  
33  
34  
35

36 Regarding the room-temperature mechanical properties, a decrease in Vickers  
37 hardness is found when increasing the SWNTs content (figure 6). The same behaviour  
38 has been recently reported in fully densified MWNT-3YTZP composites<sup>23,24</sup>. Although  
39 this tendency is usually linked to a decrease in the composite density<sup>13,25,27</sup>, the SWNT-  
40 3YTZP composites studied in this work are fully densified, denoting the decrease in  
41 hardness when increasing the CNTs content as an intrinsic effect of the CNT-3YTZP  
42 system probably associated to weak interfacial bonding between SWNTs and ceramic  
43 grains.  
44  
45  
46  
47  
48  
49  
50  
51  
52  
53  
54

55 SEM micrographs of the Vickers indentations performed in the studied  
56 composites are shown in figure 7. Values of fracture toughness obtained from these  
57  
58  
59  
60  
61  
62  
63  
64  
65

1 measurements as a function of SWNT content are shown in figure 6. Lower fracture  
2 toughness is obtained for the composites when compared to monolithic ceramic. On the  
3  
4 other hand, no significant effect of the difference in SWNT content on the fracture  
5 toughness value is observed. This result is in disagreement with the increase of fracture  
6  
7 toughness in SWNT-3YTZP composites recently reported by Shin and Hong<sup>27</sup>.  
8  
9 However, it should be noted that these authors used lower SWNT content (up to 1.0 wt  
10  
11 %) than the ones used in the present study (up to 10 vol %) to reinforce the 3YTZP  
12  
13 ceramic matrix. A similar reinforcing effect has been reported also in MWNT-3YTZP  
14  
15 composites, with an increase of fracture toughness for low CNT contents followed by a  
16  
17 decrease for high CNT contents<sup>11,15,23,25</sup>. **A comparative of the relative toughness**  
18  
19 **variation reported in literature for different CNT-3YTZP composites, according to**  
20  
21 **the type and CNT content used, relative density and zirconia grain size, is shown in**  
22  
23 **table 2.**  
24  
25  
26  
27  
28  
29  
30

31 Some authors have reported that large quantities of SWNTs would impede the  
32 densification process, leading to possible residual porosity and a subsequent decrease in  
33  
34 mechanical properties<sup>13,25,27</sup>. Also, it is widely accepted that polycrystalline tetragonal  
35  
36 zirconia compositions exhibit a substantial decrease in the contribution of  
37  
38 transformation toughening to the fracture toughness with decrease in grain size<sup>38</sup>.  
39  
40 However, the decrease of fracture toughness in the composites under study can not be  
41  
42 related to factors as possible residual porosity or smaller mean grain size with respect to  
43  
44 the monolithic ceramic, as it has been shown that all the processed samples are fully  
45  
46 dense and no significant differences were detected in grain size between the monolithic  
47  
48 ceramic and the composites (Table 1).  
49  
50  
51  
52  
53  
54

55 The classical toughening mechanisms described for conventional ceramic  
56  
57 composites reinforced by fibers or whiskers, such as fiber pull-out, crack deflection and  
58  
59  
60  
61  
62  
63  
64  
65

1 crack bridging, have been mentioned in literature as useful to describe toughening in  
2 CNT-ceramic matrix composites<sup>10,39,40</sup>. However, another possible mechanism based in  
3  
4 uncoiling and stretching of CNTs has been recently described as responsible of  
5  
6 enhanced toughness in these composites<sup>2,9</sup>. What appears to occur in this mechanism is  
7  
8 the uncoiling of the CNTs bundles located at the ceramic grain boundaries in the crack  
9  
10 wake as the crack advances intergranularly. With further propagation of the crack, the  
11  
12 uncoiled CNTs would stretch, producing crack bridging. The uncoiling and stretching  
13  
14 produces friction work and dissipates energy at the crack tip, resulting in higher  
15  
16 toughness<sup>2,9</sup>.  
17  
18  
19  
20

21  
22 In the SEM micrographs of the 3YTZP/5 vol% SWNTs composite fracture  
23  
24 surface, SWNT bridging between ceramic grains could be found (figure 4d). SWNTs  
25  
26 with two ends embedded in two separate grains are clearly observed. This observation is  
27  
28 in line with previous findings in CNT ceramic and glass composites<sup>9,23-25,40</sup>. However,  
29  
30 these SWNT bridging were scarcely found in our composites.  
31  
32

33  
34 Considering that evidences of toughening mechanisms have not been detected  
35  
36 and taking into account that the SWNT volume fraction used in this study is higher than  
37  
38 the ones used by other authors<sup>27</sup>, it could be concluded that the SWNT amounts used in  
39  
40 this study exceed the appropriate percentages that would result in an enhancement of  
41  
42 fracture toughness.  
43  
44

45  
46 Using the model developed by Zapata-Solvas et al<sup>41</sup>, it is possible to calculate  
47  
48 the surface fraction of ceramic grains in contact with SWNTs,  $A$ , for the values of  
49  
50 studied SWNT volume fractions according to:  
51  
52

$$53 A = \frac{f(1-f)d}{4w} \quad (3)$$

54  
55  
56  
57  
58  
59  
60  
61  
62  
63  
64  
65

1  
2  
3  
4  
5  
6  
7  
8  
9  
10  
11  
12  
13  
14  
15  
16  
17  
18  
19  
20  
21  
22  
23  
24  
25  
26  
27  
28  
29  
30  
31  
32  
33  
34  
35  
36  
37  
38  
39  
40  
41  
42  
43  
44  
45  
46  
47  
48  
49  
50  
51  
52  
53  
54  
55  
56  
57  
58  
59  
60  
61  
62  
63  
64  
65

Considering an estimated mean SWNT bundle diameter  $w$  of about 25 nm<sup>42</sup> and mean grain size  $d \sim 250$  nm, we obtain that 22, 12 and 6% of surface fraction of ceramic grains are covered by SWNTs for compositions with 10, 5 and 2.5 vol% SWNTs, respectively. Those percentages are clearly above percolation<sup>41</sup>. Also, this calculation reveals that the processing route used to prepare the composites gives place to a low coverage of the ceramic grains due to the existence of thick SWNT bundles (about 15 SWNTs each), which would result in a poor reinforcing effect in any case.

The accumulation of SWNT at the grain boundaries in form of thick bundles would not allow the uncoiling and stretching of SWNT when the crack is advancing but it would result in a decrease in cohesion between ceramic grains. Moreover, inter bundles detachment would be favoured rather than uncoiling and stretching, being the decohesion between SWNT within the bundle the key point in the process. 3 point bending tests carried out in SWNT solids<sup>43</sup> revealed that failure occurred via inter-bundles slippage rather than the failure of the SWNTs themselves.

Taking into account the mechanism proposed above, the fact that the SWNT contents in our composites are higher than the percolation limit would explain that the fracture toughness values are independent of the SWNT vol%.

Future work will be performed to clarify whether a toughness enhancement mechanism exists in low SWNT content composites, in order to assess if lower SWNT vol% results in thinner SWNT bundles surrounding the ceramic grains and that finally results in an enhancement of the mechanical properties of the composite.

#### 4. Conclusions

1 Fully dense 3 mol% yttria doped zirconia matrix composites containing 2.5, 5  
2 and 10 vol% SWNT have been prepared by using a combination of aqueous colloidal  
3 powder processing and Spark Plasma Sintering. All the samples are mainly tetragonal,  
4 with a minor contribution of the monoclinic phase. An increase of the latter when  
5 increasing the SWNT content was found, pointing to a transformation of the tetragonal  
6 phase to the monoclinic one promoted by the presence of SWNTs.  
7  
8  
9  
10  
11  
12  
13

14 An equiaxed grain microstructure and an almost constant ceramic grain size  
15 (190-270 nm) have been obtained in the composites. SWNTs were located on the  
16 ceramic grain boundaries and homogeneously distributed on the ceramic matrix at the  
17 nanoscale, however, the presence of large SWNT agglomerates could not be avoided.  
18  
19  
20  
21  
22  
23

24 A decrease in hardness has been found when increasing the SWNTs content in  
25 spite of the full densification of the composites. A decrease of the fracture toughness  
26 was also found, possibly as a consequence of a SWNT weakening effect on interfacial  
27 cohesion between ceramic grains. The detachment between SWNT within bundles has  
28 been pointed out as the decisive point in the fracture process.  
29  
30  
31  
32  
33  
34  
35  
36  
37  
38

### 39 **Acknowledgements**

40  
41  
42 The financial support for this work has been obtained from the Spanish Ministry of  
43 Science and Innovation (MAT2012-34217) and from Junta de Andalucía (P12-FQM-  
44 1079). XRD and microscopy studies have been performed in facilities belonging to the  
45 CITIUS (Universidad de Sevilla). Prof. F.L. Cumbreira (Univ. of Sevilla) is greatly  
46 acknowledged for the Rietveld refinement.  
47  
48  
49  
50  
51  
52  
53  
54  
55  
56  
57  
58  
59  
60  
61  
62  
63  
64  
65

## References

- <sup>1</sup> J. Cho, A.R. Boccaccini, M.S.P. Shaffer, Ceramic matrix composites containing carbon nanotubes, *J. Mater. Sci.* 44 (2009) 1934-51.
- <sup>2</sup> N.P. Padture, Multifunctional composites of ceramics and single-walled Carbon nanotubes, *Adv. Mater.* 21 (2009) 1767–70.
- <sup>3</sup> P.J.F. Harris, Carbon nanotube composites, *Int. Mater. Rev.* 49 (2004) 31-43.
- <sup>4</sup> S. Iijima, C.H. Brabec, A. Maiti, Z.J. Bernholc, Structural flexibility of carbon nanotubes, *J. Chem. Phys.* 104 (1996) 2089–92.
- <sup>5</sup> R.H. Baughman, A.A. Zakhidov, W.A. Heer, Carbon nanotubes- The route toward applications, *Science* 297 (2002) 787–92.
- <sup>6</sup> G.D. Zhan, J.D. Kuntz, J. Wan, A.K. Mukherjee, Single-wall carbon nanotubes as attractive toughening agents in alumina based nanocomposites, *Nat. Mater.* 2 (2003) 38-42.
- <sup>7</sup> E. Zapata-Solvas, R. Poyato, D. Gómez-García, A. Domínguez-Rodríguez, V. Radmilovic, N.P. Padture, Creep-resistant composites of alumina and single-wall carbon nanotubes, *Appl. Phys. Lett.* 92 (2008) 111912.
- <sup>8</sup> M. Mazaheri, D. Mari, R. Schaller, G. Bonfont, G. Fantozzi, Processing of yttria stabilized zirconia reinforced with multi-walled carbon nanotubes with attractive mechanical properties, *J. Eur. Ceram. Soc.* 31 (2011) 2691-98.
- <sup>9</sup> M. Mazaheri, D. Mari, Z. Razavi Hesabi, R. Schaller, G. Fantozzi, Multi-walled carbon nanotube/nanostructured zirconia composites: Outstanding mechanical properties in a wide range of temperature, *Composites Sci. Technol.* 71 (2011) 939-45.
- <sup>10</sup> I. Ahmad, H. Cao, H. Chen, H. Zhao, A. Kennedy, Y.Q. Zhu, Carbon nanotube toughened aluminum oxide nanocomposite, *J. Eur. Ceram. Soc.* 30 (2010) 865-873.



- 
- 1 <sup>11</sup> T. Ukai, T. Sekino, A. Hirvonen, N. Tanaka, T. Kusunose, T. Nakayama, K. Niihara,  
2  
3 Preparation and electrical properties of carbon nanotubes dispersed zirconia  
4  
5 nanocomposites, *Key Eng. Mater.* 317-318 (2006) 661-64.  
6  
7  
8 <sup>12</sup> X. Wang, N.P. Padture, H. Tanaka, Contact-damage-resistant ceramic/single-wall  
9  
10 carbon nanotubes and ceramic/graphite composites, *Nat. Mater.* 3 (2004) 539-44.  
11  
12  
13 <sup>13</sup> A. Duszová, J. Dusza, K. Tomasek, G. Blugan, J. Kuebler, Microstructure and  
14  
15 properties of carbon nanotube/zirconia composite, *J. Eur. Ceram. Soc.* 28 (2008) 1023-  
16  
17 27.  
18  
19  
20 <sup>14</sup> N. Garmendia, I. Santacruz, R. Moreno, I. Obieta, Slip casting of  
21  
22 nanozirconia/MWCNT composites using a heterocoagulation process, *J. Eur. Ceram.*  
23  
24 *Soc.* 29 (2009) 1939-45.  
25  
26  
27 <sup>15</sup> J. Sun, L. Gao, M. Iwasa, T. Nakayama, K. Niihara, Failure investigation of carbon  
28  
29 nanotube/3Y-TZP nanocomposites, *Ceram. Int.* 31 (2005) 1131–1134.  
30  
31  
32 <sup>16</sup> R. Poyato, A.L. Vasiliev, N.P. Padture, H. Tanaka, T. Nishimura, Aqueous colloidal  
33  
34 processing of single-wall carbon nanotubes and their composites with ceramics,  
35  
36 *Nanotech.* 17 (2006) 1770–1777.  
37  
38  
39  
40 <sup>17</sup> M. Poorteman, M. Traianidis, G. Bister, F. Cambier, Colloidal processing, hot  
41  
42 pressing and characterisation of electroconductive MWCNT-alumina composites with  
43  
44 compositions near the percolation threshold, *J. Eur. Ceram. Soc.* 29 (2009) 669-675.  
45  
46  
47 <sup>18</sup> T. Zhang, L. Kumari, G.H. Du, W.Z. Li, Q.W. Wang, K. Balani, A. Agarwal,  
48  
49 Mechanical properties of carbon nanotube–alumina nanocomposites synthesized by  
50  
51 chemical vapor deposition and spark plasma sintering, *Compos: Part A* 40 (2009) 86–  
52  
53 93.  
54  
55  
56  
57 <sup>19</sup> A. Datye, K.H. Wu, G. Gomes, V. Monroy, H.T. Lin, J. Vleugels, K. Vanmeensel,  
58  
59 Synthesis, microstructure and mechanical properties of yttria stabilized zirconia  
60  
61  
62  
63  
64  
65

---

1 (3YTZP)-multi-walled nanotube (MWNTs) nanocomposite by direct in-situ growth of  
2  
3 MWNTs on zirconia particles, *Composites Sci. Technol.* 70 (2010) 2086-92.

4  
5  
6 <sup>20</sup> N.Q. Minh, Ceramic fuel cells, *J. Am. Ceram. Soc.* 76 (1993) 563–588.

7  
8  
9  
10  
11 <sup>21</sup> W.C. Maskell, Progress in the development of zirconia gas sensors, *Solid State Ion.*  
12 134 (2000) 43-50.

13  
14  
15  
16  
17  
18  
19 <sup>22</sup> S. Deville, L. Gremillard, J. Chevalier, G. Fantozzi, A critical comparison of methods  
20 for the determination of the aging sensitivity in biomedical grade yttria-stabilized  
21 zirconia, *J. Biomed. Mater. Res. B: Appl. Biomater.* 72 (2005) 239-45.

22  
23  
24  
25  
26  
27 <sup>23</sup> N. Garmendia, S. Grandjean, J. Chevalier, L.A. Diaz, R. Torrecillas, I. Objeta,  
28 Zirconia-multiwall carbon nanotubes dense nano-composites with an unusual balance  
29 between crack and ageing resistance, *J. Eur. Ceram. Soc.* 31 (2011) 1009-14.

30  
31  
32  
33  
34  
35  
36 <sup>24</sup> R.K. Chintapalli, F. Garcia Marro, B. Milsom, M. Reece, M. Anglada, Processing and  
37 characterization of high-density zirconia-carbon nanotube composites, *Mater. Sci. Eng.*  
38 A 549 (2012) 50-59.

39  
40  
41  
42  
43  
44  
45  
46  
47  
48  
49  
50  
51 <sup>25</sup> J.P. Zhou, Q.M. Gong, K.Y. Yuan, J.J. Wu, Y.F. Chen, C.S. Li, J. Liang, The effects  
52 of multiwalled carbon nanotubes on the hot-pressed 3 mol% yttria stabilized zirconia  
53 ceramics, *Mater. Sci. Eng. A* 520 (2009) 153-57.

54  
55  
56  
57  
58  
59  
60  
61  
62  
63  
64  
65 <sup>26</sup> M.H. Bocanegra-Bernal, J. Echeberria, J. Ollo, A. Garcia-Reyes, Domínguez-Rios, A.  
66 Reyes-Rojas, A. Aguilar-Elguezabal, A comparison of the effects of multi-wall and  
67 single-wall carbon nanotube additions on the properties of zirconia toughened alumina  
68 composites, *Carbon* 49 (2011) 1599-1607.

69  
70  
71  
72  
73  
74  
75  
76  
77  
78  
79  
80  
81  
82  
83  
84  
85  
86  
87  
88  
89  
90  
91  
92  
93  
94  
95  
96  
97  
98  
99  
100  
<sup>27</sup> J.H. Shin, S.H. Hong, Microstructure and mechanical properties of single wall carbon  
nanotube reinforced yttria stabilized zirconia ceramics, *Mater. Sci. Eng. A* 556 (2012)  
382-87.

- 
- 1       <sup>28</sup> D. Jiang, K. Thomson, J.D. Kuntz, J.W. Ager, A.K. Mukherjee, Effect of sintering  
2  
3 temperature on a single-wall carbon nanotube-toughened alumina-based nanocomposite,  
4  
5 *Scripta Mater.* 56 (2007) 959-62.  
6  
7  
8       <sup>29</sup> N.P. Padture, W.A. Curtin, Comment on “Effect of sintering temperature on a single-  
9  
10 wall carbon nanotube-toughened alumina-based nanocomposite”, *Scripta Mater.* 58  
11  
12 (2008) 989-90.  
13  
14  
15       <sup>30</sup> D. Jiang, A.K. Mukherjee, Response to comment on “Effect of sintering temperature  
16  
17 on a single-wall carbon nanotube-toughened alumina-based nanocomposite”, *Scripta*  
18  
19 *Mater.* 58 (2008) 991-93.  
20  
21  
22       <sup>31</sup> J. Cho, F. Inam, M.J. Reece, Z. Chlup, I. Dlouhy, M.S.P. Shaffer, A.R. Boccaccini,  
23  
24 Carbon nanotubes: do they toughen brittle matrices?, *J. Mater. Sci.* 46 (2011) 4770-79.  
25  
26  
27       <sup>32</sup> J. Liu, A.G. Rinzler, H. Dai, J.H. Hafner, R.K. Bradley, P.J. Boul, A. Lu, T. Iverson,  
28  
29 K. Shelimov, C.B. Huffman, F. Rodríguez-Macías, Y.S. Shon, T.R. Lee, D.T. Colbert,  
30  
31 R.E. Smalley, Fullerene Pipes, *Science* 280 (1998) 1253-56.  
32  
33  
34       <sup>33</sup> G.R. Anstis, P. Chantikul, D.B. Lawn, D.B. Marshall, A critical evaluation of  
35  
36 indentation techniques for measuring fracture toughness: I. direct crack measurement, *J.*  
37  
38 *Am. Ceram. Soc.* 64 (1981) 533–38.  
39  
40  
41       <sup>34</sup> M.H. Bocanegra-Bernal, A. Reyes-Rojas, A. Aguilar-Elguezabal, E. Torres-Moye, J.  
42  
43 Echeberria, X-ray diffraction evidence of a phase transformation in zirconia by the  
44  
45 presence of graphite and carbon nanotubes in zirconia toughened alumina composites,  
46  
47 *Int. J. Ref. Metals Hard Mater.* 35 (2012) 315-18.  
48  
49  
50       <sup>35</sup> P.M. Ajayan, L.S. Schadler, C. Giannaris, A. Rubio, Single-walled carbon nanotube-  
51  
52 polymer composites: Strength and weakness, *Adv. Mater.* 12 (2000) 750–3.  
53  
54  
55  
56  
57  
58  
59  
60  
61  
62  
63  
64  
65

- 
- 1 <sup>36</sup> M. Li, Z. Feng, G. Xiang, P. Ying, Q. Xin, C. Li, Phase Transformation in the Surface  
2  
3 Region of Zirconia Detected by UV Raman Spectroscopy, *J. Phys. Chem. B* 105 (2001)  
4  
5 8107–11.  
6  
7  
8 <sup>37</sup> S.A. Cruz, R. Poyato, F.L. Cumbreira, J.A. Odriozola, Nanostructured Spark Plasma  
9  
10 Sintered Ce-TZP Ceramics, *J. Am. Ceram. Soc.* 95 (2012) 901–906.  
11  
12  
13 <sup>38</sup> P.F. Bechar and M.V. Swain, Grain-size-dependent transformation behaviour in  
14  
15 polycrystalline tetragonal zirconia, *J. Am. Ceram. Soc.* 75 (1992) 493-502.  
16  
17  
18 <sup>39</sup> Z. Xia, L. Riester, W.A. Curtin, H. Li, B.W. Sheldon, J. Liang, B. Chang, J.M. Xu,  
19  
20 Direct observation of toughening mechanisms in carbon nanotube ceramic matrix  
21  
22 composites, *Acta Mater.* 52 (2004) 931–44.  
23  
24  
25 <sup>40</sup> A. Mukhopadhyay, B.T.T. Chu, M.L.H. Green, R.I. Todd, Understanding the  
26  
27 mechanical reinforcement of uniformly dispersed multiwalled carbon nanotubes in  
28  
29 alumino-borosilicate glass ceramic, *Acta Mater.* 58 (2010) 2685–97.  
30  
31  
32 <sup>41</sup> E. Zapata-Solvas, D. Gómez-García, A. Domínguez-Rodríguez, On the  
33  
34 microstructure of single wall carbon nanotubes reinforced ceramic matrix composites, *J.*  
35  
36 *Mater. Sci.* 45 (2012) 2258-63.  
37  
38  
39 <sup>42</sup> E. Zapata-Solvas, D. Gómez-García, A. Domínguez-Rodríguez, Towards physical  
40  
41 properties tailoring of carbon nanotubes-reinforced ceramic matrix composites, *J. Eur.*  
42  
43 *Ceram. Soc.* 32 (2012) 3001-3020.  
44  
45  
46 <sup>43</sup> G. Yamamoto, Y. Sato, T. Takahashi, M. Omori, T. Hashida, A. Okubo, K. Tohji,  
47  
48 Single-walled carbon nanotube-derived novel structural material, *J. Mater. Res.* 21  
49  
50 (2006) 1537-1542.  
51  
52  
53  
54  
55  
56  
57  
58  
59  
60  
61  
62  
63  
64  
65

## Figure captions

**Figure 1:** Shrinkage and temperature curves recorded during the SPS processing of the 3YTZP/SWNTs composites.

**Figure 2:** X-ray diffraction patterns of the monolithic 3YTZP ceramic and the composites.

**Figure 3:** Raman spectra measured in the composites including the RBM frequency range, and the D-Band and G-Band frequency range. Raman spectra measured in the monolithic 3YTZP ceramic and in the SWNTs have been included for comparison.

**Figure 4:** HRSEM micrographs of fracture surface of the composites reinforced with different SWNT contents (a) and (b) 2.5 vol%, (c) and (d) 5 vol%, and (e) and (f) 10 vol%.

**Figure 5:** HRSEM micrographs of thermally etched polished surfaces and grain size distribution plots of the (a) monolithic 3YTZP ceramic, and (b) composite reinforced with 5 vol% SWNTs. (c) HRSEM micrographs of thermally etched polished surface of the 3YTZP/5 vol% SWNTs composite, showing some holes related to agglomerates burned out during thermal etching in air.

**Figure 6:** Hardness and indentation fracture toughness of the SWNT-3YTZP composites.

\*Corresponding author. E-mail address: [rosalia.poyato@icmse.csic.es](mailto:rosalia.poyato@icmse.csic.es)

Phone number: +34 954 48 95 34

FAX number: +34 954 46 06 65

**Figure 7:** SEM micrographs of the Vickers indentations in the composites with (a) 2.5, (b) 5, and (c) 10 vol% SWNTs.

1  
2  
3  
4  
5  
6  
7  
8  
9  
10  
11  
12  
13  
14  
15  
16  
17  
18  
19  
20  
21  
22  
23  
24  
25  
26  
27  
28  
29  
30  
31  
32  
33  
34  
35  
36  
37  
38  
39  
40  
41  
42  
43  
44  
45  
46  
47  
48  
49  
50  
51  
52  
53  
54  
55  
56  
57  
58  
59  
60  
61  
62  
63  
64  
65

**Table 1:** Properties of the studied composites

<b>Material</b>	<b>Relative density (%)</b>	<b>Grain size (<math>\mu\text{m}</math>)</b>	<b>F</b>	<b>Hardness (GPa)</b>	<b>Fracture toughness (<math>\text{MPa}\cdot\text{m}^{1/2}</math>)</b>
<b>3YTZP</b>	<b>100</b>	$0.26 \pm 0.11$	$0.76 \pm 0.06$	$13.0 \pm 0.5$	$6.1 \pm 0.9$
<b>3YTZP/2.5 vol% SWNT</b>	<b>100</b>	$0.27 \pm 0.13$	$0.76 \pm 0.06$	$12.4 \pm 0.7$	$4.7 \pm 0.9$
<b>3YTZP/5 vol% SWNT</b>	<b>99.3</b>	$0.19 \pm 0.08$	$0.76 \pm 0.07$	$11.4 \pm 0.5$	$4.8 \pm 0.6$
<b>3YTZP/10 vol% SWNT</b>	<b>100</b>	$0.24 \pm 0.13$	$0.76 \pm 0.08$	$9.2 \pm 0.9$	$5.0 \pm 0.8$

**Table 2: Comparison of properties for CNT-3YTZP composites reported in literature.**

	Type of CNT	CNT vol%	Grain size (nm)	Relative Density (%)	Method of $K_{IC}$ measurement	$K_{IC}$ (MPa·m <sup>1/2</sup> )		Relative $K_{IC}$ variation (%)
						Monolithic	Composite	
<b>This study</b>	<b>SWNT</b>	<b>2.5</b>	<b>270</b>	<b>100</b>	<b>IF</b>	<b>6.1</b>	<b>4.7</b>	<b>-23</b>
<b>Shin 2012 (27)</b>	<b>SWNT</b>	<b>3.4</b>	<b>280</b>	<b>98.0</b>	<b>IF</b>	<b>4.4</b>	<b>5.2</b>	<b>18</b>
<b>Chintapalli 2012 (24)</b>	<b>MWNT</b>	<b>2</b>	<b>161</b>	<b>98.7</b>	<b>IF</b>	<b>3.9</b>	<b>4.5</b>	<b>15</b>
<b>Garmendia 2011 (23)</b>	<b>MWNT</b>	<b>3</b>	<b>218</b>	<b>99.5</b>	<b>IF</b>	<b>2.36</b>	<b>4.06</b>	<b>72</b>
		<b>6</b>	<b>146</b>	<b>99.1</b>	<b>IF</b>	<b>2.36</b>	<b>2.07</b>	<b>-14</b>
<b>Mazaheri 2011 (9)</b>	<b>MWNT</b>	<b>12.5</b>	<b>96</b>	<b>98.4</b>	<b>IF</b>	<b>5.5</b>	<b>11</b>	<b>100</b>
					<b>SENB</b>	<b>6</b>	<b>8</b>	<b>33</b>
<b>Zhou 2009 (25)</b>	<b>MWNT</b>	<b>3.4</b>	<b>---</b>	<b>98.6</b>	<b>IF</b>	<b>4.9</b>	<b>5.8</b>	<b>21</b>
		<b>5</b>	<b>---</b>	<b>98</b>	<b>IF</b>	<b>4.9</b>	<b>5.2</b>	<b>5</b>
<b>Garmendia 2009</b>	<b>MWNT</b>	<b>1</b>	<b>220</b>	<b>95.7</b>	<b>IF</b>	<b>3.8</b>	<b>4.0</b>	<b>5</b>
<b>Duszová 2008 (13)</b>	<b>MWNT</b>	<b>3.4</b>	<b>140</b>	<b>88</b>	<b>IF</b>	<b>6.24</b>	<b>5.6</b>	<b>-10</b>
<b>Ukai 2006 (11)</b>	<b>MWNT</b>	<b>1.7</b>	<b>---</b>	<b>100</b>	<b>IF</b>	<b>5.56</b>	<b>6.10</b>	<b>10</b>
		<b>3.4</b>	<b>---</b>	<b>100</b>	<b>IF</b>	<b>5.56</b>	<b>5.69</b>	<b>2</b>
<b>Sun 2005 (15)</b>	<b>MWNT</b>	<b>1.7</b>	<b>---</b>	<b>99.1</b>	<b>IF</b>	<b>5.28</b>	<b>5.52</b>	<b>4</b>
		<b>3.4</b>	<b>---</b>	<b>99.1</b>	<b>IF</b>	<b>5.28</b>	<b>4.47</b>	<b>-15</b>

**\* IF: Indentation Fracture, SENB: Single Edge Notched Beam**



**Table 1:** Properties of the studied composites

<b>Material</b>	<b>Relative density (%)</b>	<b>Grain size (<math>\mu\text{m}</math>)</b>	<b>F</b>	<b>Hardness (GPa)</b>	<b>Fracture toughness (<math>\text{MPa}\cdot\text{m}^{1/2}</math>)</b>
<b>3YTZP</b>	100	$0.26 \pm 0.11$	$0.76 \pm 0.06$	$13.0 \pm 0.5$	$6.1 \pm 0.9$
<b>3YTZP/2.5 vol% SWNT</b>	100	$0.27 \pm 0.13$	$0.76 \pm 0.06$	$12.4 \pm 0.7$	$4.7 \pm 0.9$
<b>3YTZP/5 vol% SWNT</b>	99.3	$0.19 \pm 0.08$	$0.76 \pm 0.07$	$11.4 \pm 0.5$	$4.8 \pm 0.6$
<b>3YTZP/10 vol% SWNT</b>	100	$0.24 \pm 0.13$	$0.76 \pm 0.08$	$9.2 \pm 0.9$	$5.0 \pm 0.8$

**Table 2:** Comparison of properties for CNT-3YTZP composites reported in literature.

	Type of CNT	CNT vol%	Grain size (nm)	Relative Density (%)	Method of $K_{IC}$ measurement	$K_{IC}$ (MPa·m <sup>1/2</sup> )		Relative $K_{IC}$ variation (%)
						Monolithic	Composite	
This study	SWNT	2.5	270	100	IF	6.1	4.7	-23
Shin 2012 (27)	SWNT	3.4	280	98.0	IF	4.4	5.2	18
Chintapalli 2012 (24)	MWNT	2	161	98.7	IF	3.9	4.5	15
Garmendia 2011 (23)	MWNT	3	218	99.5	IF	2.36	4.06	72
		6	146	99.1	IF	2.36	2.07	-14
Mazaheri 2011 (9)	MWNT	12.5	96	98.4	IF	5.5	11	100
					SENB	6	8	33
Zhou 2009 (25)	MWNT	3.4	---	98.6	IF	4.9	5.8	21
		5	---	98	IF	4.9	5.2	5
Garmendia 2009	MWNT	1	220	95.7	IF	3.8	4.0	5
Duszová 2008 (13)	MWNT	3.4	140	88	IF	6.24	5.6	-10
Ukai 2006 (11)	MWNT	1.7	---	100	IF	5.56	6.10	10
		3.4	---	100	IF	5.56	5.69	2
Sun 2005 (15)	MWNT	1.7	---	99.1	IF	5.28	5.52	4
		3.4	---	99.1	IF	5.28	4.47	-15

\* IF: Indentation Fracture, SENB: Single Edge Notched Beam

Figure 1

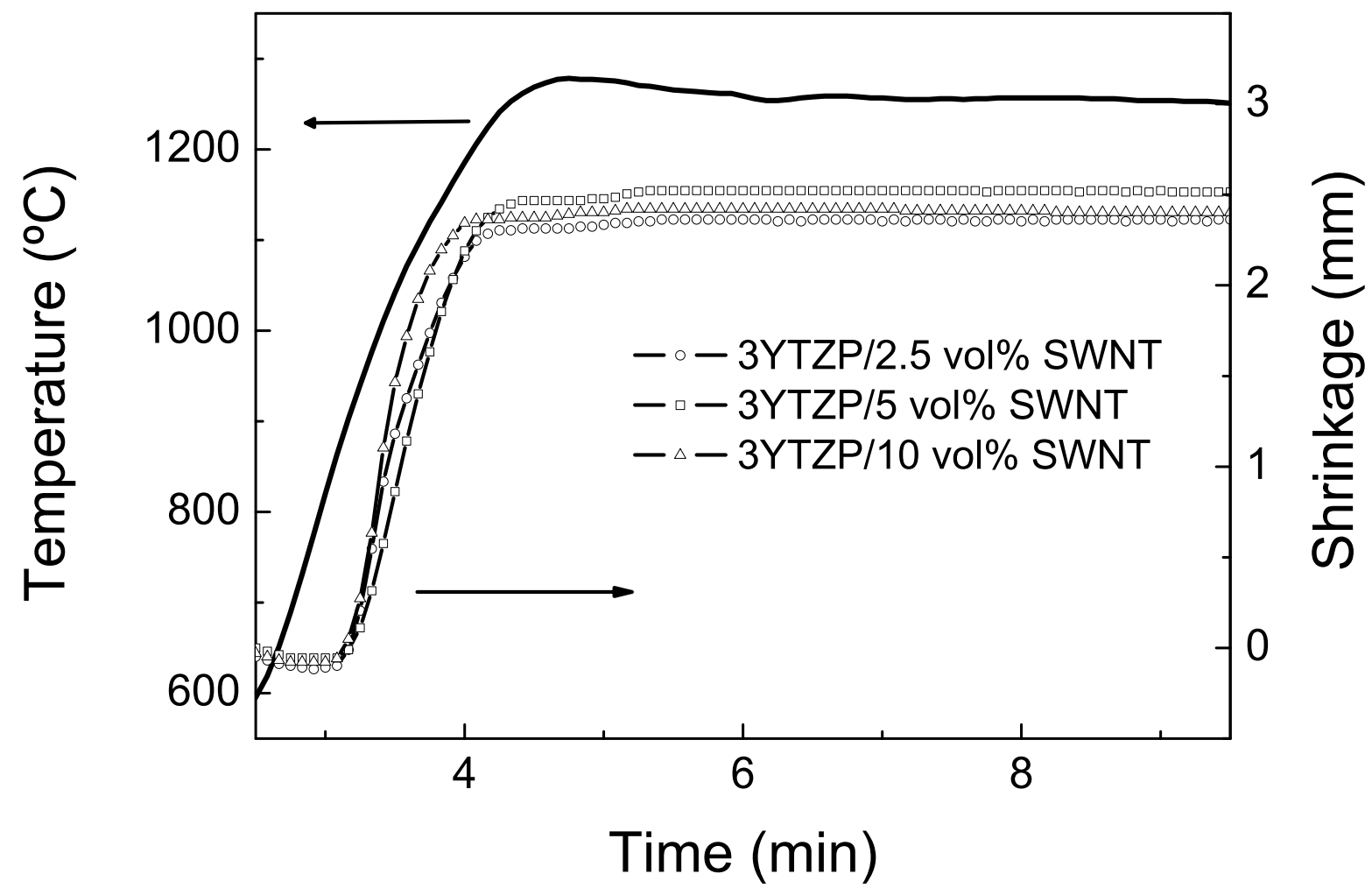


Figure 2

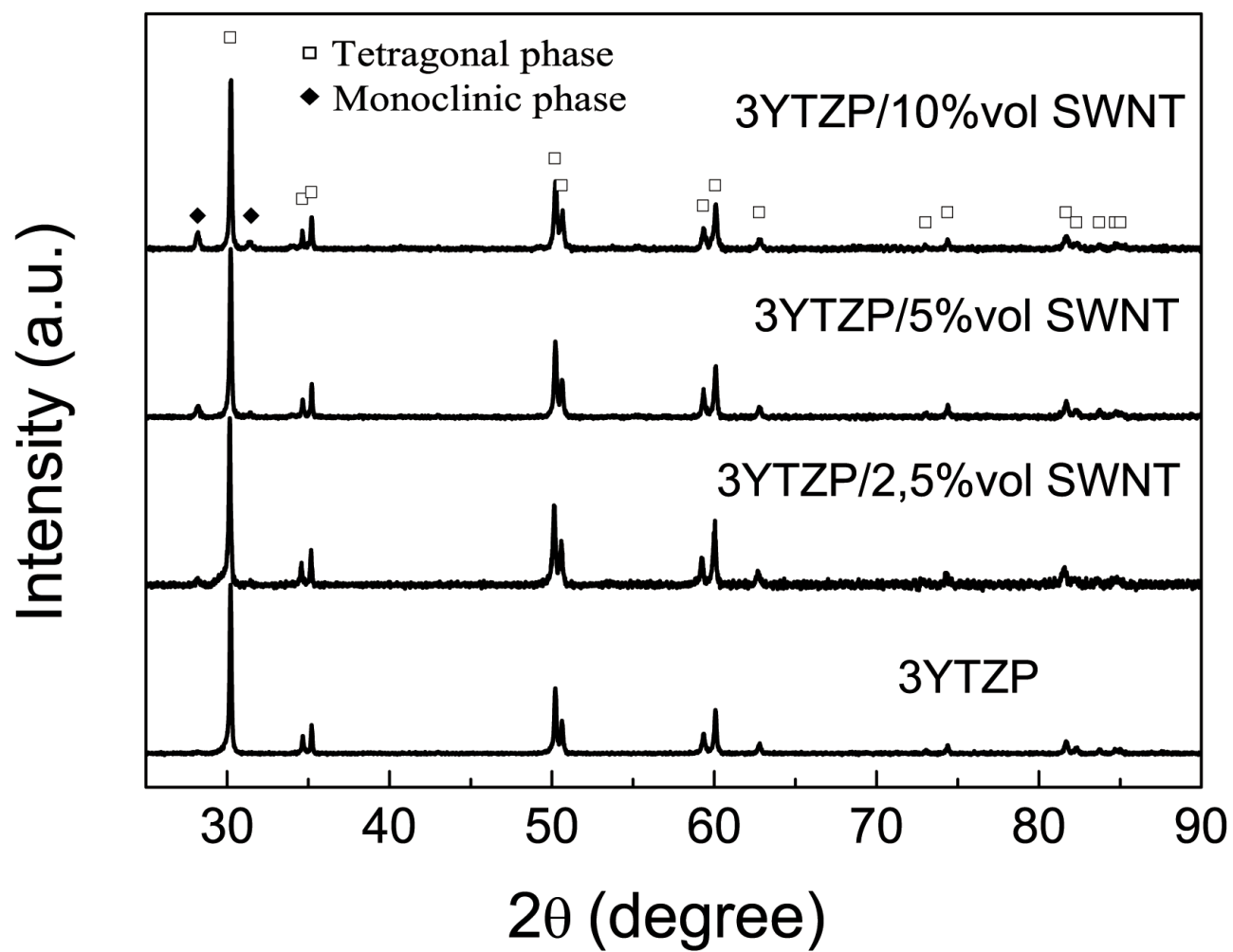


Figure 3

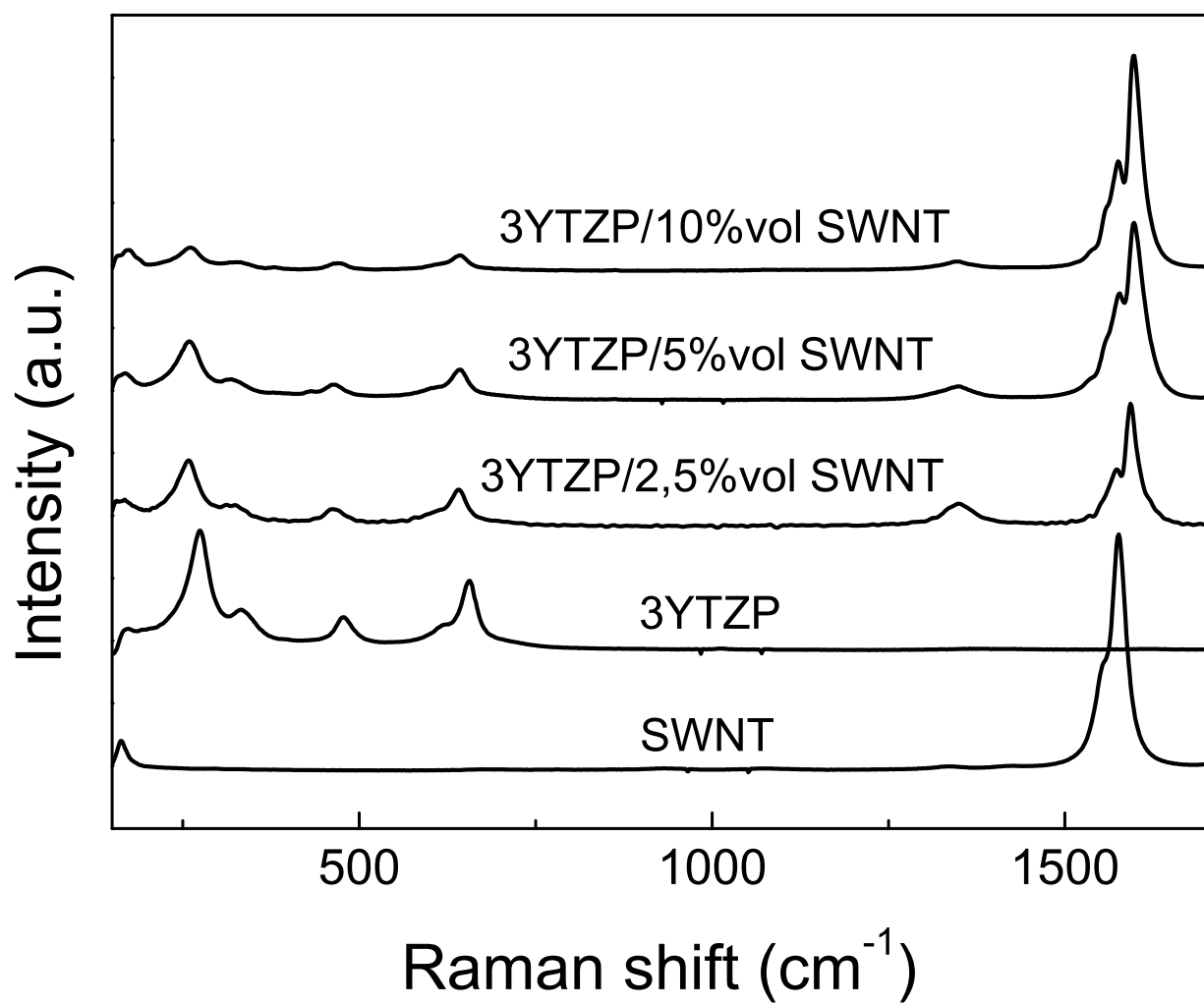


Figure 4  
[Click here to download high resolution image](#)

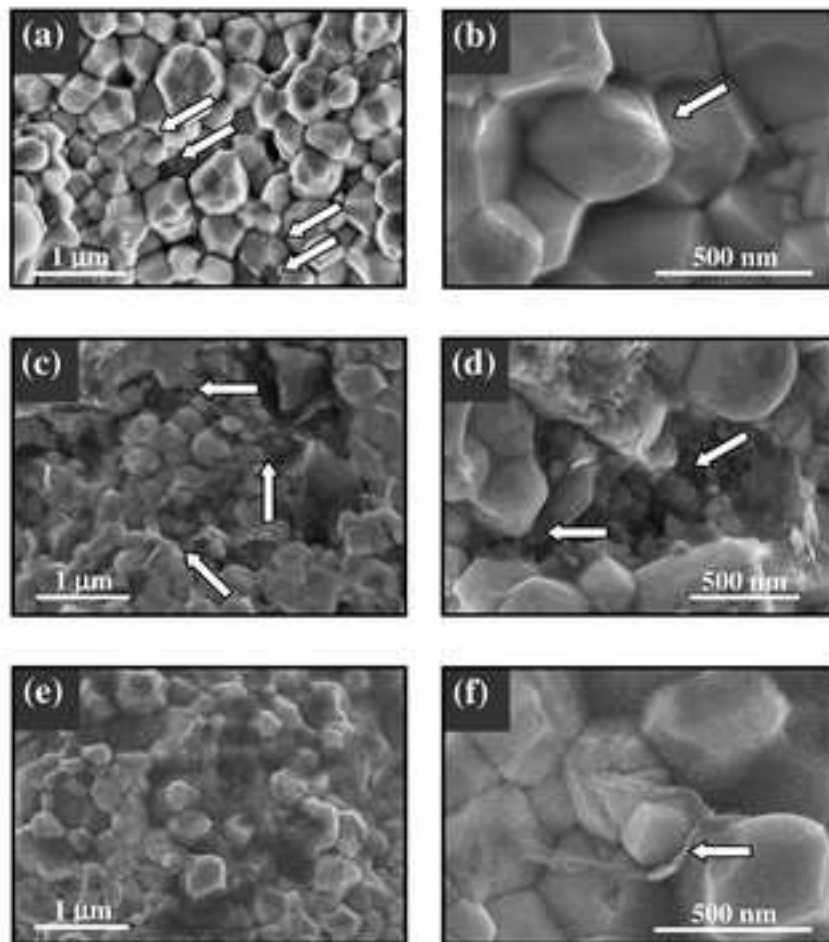


Figure 5  
[Click here to download high resolution image](#)

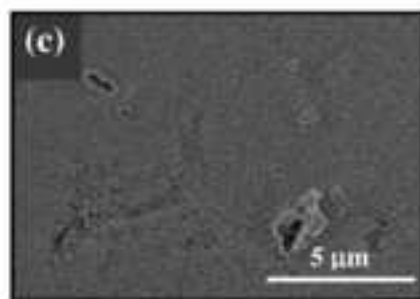
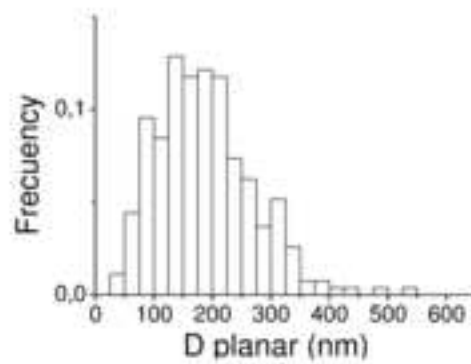
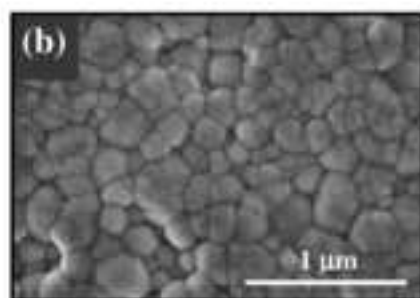
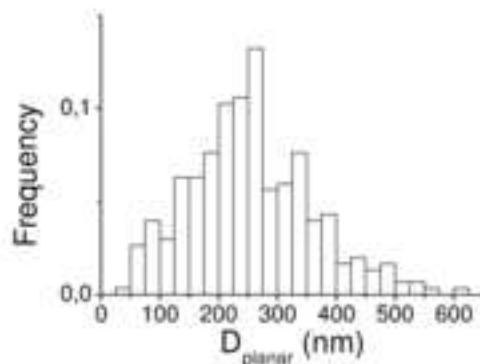
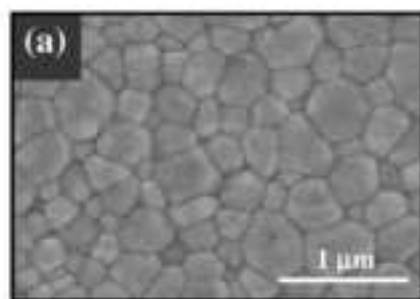
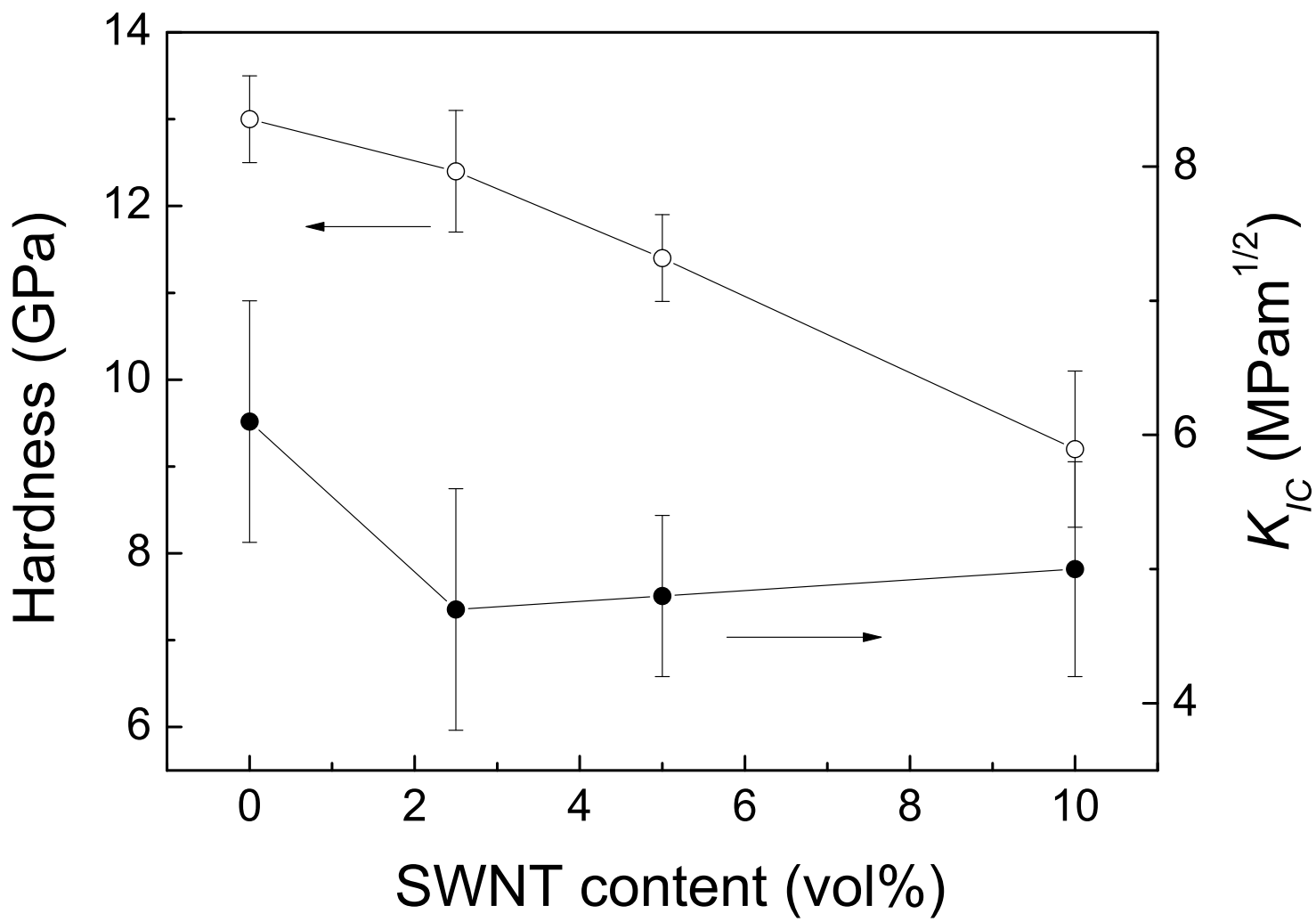


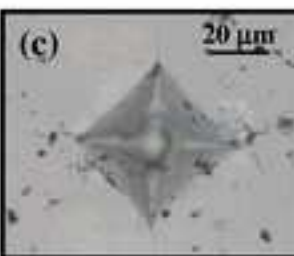
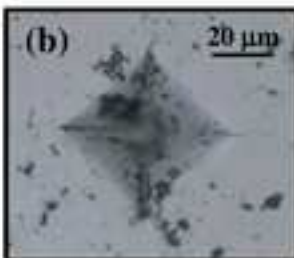
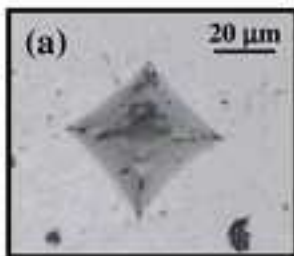
Figure 5

Figure 6





**Figure 7**  
[Click here to download high resolution image](#)



**Figure captions**

1  
2  
3  
4  
5 **Figure 1:** Shrinkage and temperature curves recorded during the SPS processing of the  
6  
7 3YTZP/SWNTs composites.  
8  
9

10  
11  
12 **Figure 2:** X-ray diffraction patterns of the monolithic 3YTZP ceramic and the  
13  
14 composites.  
15  
16

17  
18  
19 **Figure 3:** Raman spectra measured in the composites including the RBM frequency  
20  
21 range, and the D-Band and G-Band frequency range. Raman spectra measured in the  
22  
23 monolithic 3YTZP ceramic and in the SWNTs have been included for comparison.  
24  
25

26  
27  
28  
29 **Figure 4:** HRSEM micrographs of fracture surface of the composites reinforced with  
30  
31 different SWNT contents (a) and (b) 2.5 vol%, (c) and (d) 5 vol%, and (e) and (f) 10  
32  
33 vol%.  
34  
35

36  
37  
38  
39 **Figure 5:** HRSEM micrographs of thermally etched polished surfaces and grain size  
40  
41 distribution plots of the (a) monolithic 3YTZP ceramic, and (b) composite reinforced  
42  
43 with 5 vol% SWNTs. (c) HRSEM micrographs of thermally etched polished surface of  
44  
45 the 3YTZP/5 vol% SWNTs composite, showing some holes related to agglomerates  
46  
47 burned out during thermal etching in air.  
48  
49

50  
51  
52  
53 **Figure 6:** Hardness and indentation fracture toughness of the SWNT-3YTZP  
54  
55 composites.  
56  
57  
58  
59  
60  
61  
62  
63  
64  
65

**Figure 7:** SEM micrographs of the Vickers indentations in the composites with (a) 2.5, (b) 5, and (c) 10 vol% SWNTs.

1  
2  
3  
4  
5  
6  
7  
8  
9  
10  
11  
12  
13  
14  
15  
16  
17  
18  
19  
20  
21  
22  
23  
24  
25  
26  
27  
28  
29  
30  
31  
32  
33  
34  
35  
36  
37  
38  
39  
40  
41  
42  
43  
44  
45  
46  
47  
48  
49  
50  
51  
52  
53  
54  
55  
56  
57  
58  
59  
60  
61  
62  
63  
64  
65